Chinese Journal of Aeronautics 24 (2011) 136-144

Contents lists available at ScienceDirect

Chinese Journal of Aeronautics

journal homepage: www.elsevier.com/locate/cja

Numerical Simulation of 2D Supersonic Magnetohydrodynamic Channel and Study on Hall Effect

ZHENG Xiaomei, LU Haoyu, XU Dajun, CAI Guobiao*

School of Astronautics, Beihang University, Beijing 100191, China

Received 10 April 2010; revised 30 June 2010; accepted 4 December 2010

Abstract

In this research effort, numerical simulation of two-dimensional magnetohydrodynamic (MHD) channel is performed and Hall effect is studied. The computational model consists of the Navier-Stokes (N-S) equations coupled with electrical-magnetic source terms, Maxwell equations and the generalized Ohm's law. Boundary conditions for the electrical potential equation considering Hall effect are derived. To start with, the MHD channel with single-pair electrodes is studied and flow of the electric current is in accordance with physical principle. Then the MHD channel with five-pair electrodes is numerically simulated. The results show that the electrical current concentrates on the downstream of the anode and the upstream of the cathode due to Hall effect, and the flow field becomes asymmetrical. At the current value of the magnetic interaction parameter, the electrical-magnetic force affects the flow remarkably, decreasing the outlet Mach number and increasing the outlet pressure; what's more, the flow structure in the channel becomes extremely complex. Performances of MHD channels with continual electrodes and segmented electrodes are compared. The results show that performance of the MHD channel with segmented electrodes is better than that with continual electrodes with the increase of Hall parameter.

Keywords: hypersonic vehicles; scramjet; magnetohydrodynamics; Hall effect; numerical simulation

1. Introduction

Since the 1950's, applications of magnetohydrodynamic (MHD) technology on aircraft have received considerable attention. Emphases of the research were MHD shock wave control and thermal management at the front of the aircraft[1-2]. In the 1990's, a new concept of using the combined turbojet and MHD scramjet engine as power system of the hypersonic cruiser was established. The project was named as the AJAX[3] project, and the engine was called MHD controlled scramjet. The MHD controlling technology is on a new development path since then. In the AJAX program, an MHD generator is used to extract a portion of the aerodynamic heating energy from the inlet, and an MHD accelerator is used to reintroduce this power as kinetic energy to the exhaust stream. In this way, the combustor entrance Mach number and static temperature can be limited to a specific value as the flight Mach number increases.

The possibility of MHD energy bypass scramjet was analyzed using quasi-one-dimensional mathematical model by Freishtadt[4]. In the model, the gas was assumed to be inviscid, thermally nonconducting ideal and constant specific heat. The channel was assumed to be ideally segmented Faraday MHD channel. The model was quite straightforward and fit for feasibility study of first period. Kuranov, et al.[5] have done research on MHD controlled inlet with two-dimensional (2D) inviscid model consisting of the Euler equations coupled with electro-magnetic sources and generalized Ohm's law, but Hall effect and ion-slip were not considered. Golovachov, et al.[6-7] researched the problem of gas control by magnetic field in the 2D intakes of supersonic aircraft. Conductivity tensor was used to

*Corresponding author. Tel.: +86-10-82316533.
E-mail address: cgb@buaa.edu.cn

doi: 10.1016/S1000-9361(11)60017-4

solve the electrical potential equation. Wall boundary conditions for the potential equation are given by fixed values of electric field potential on the electrodes and by zero value of the electric current density normal to wall on the insulators, which was not enough when considering the Hall effect. This will be explained later. From the potential distribution figure in Ref.[6], Hall effect was not presented, and in the current distribution figure we can see that the current flows through the electrodes, insulators, inlet and outlet of the channel, which are obviously incorrect. Three-dimensional (3D) computational model was used by Gaitonde[8-10] to research the phenomenon in MHD energy bypass scramjet, conductivity tensor was used to solve the electrical potential in 3D space considering Hall effect and ion slip, and the boundary conditions for electrodes and insulators were derived for implementation on general 3D curvilinear meshes.

Lu[11] employed the five-wave MHD model covering the influences of Hall effect and ion slip to analyze the aerothermodynamic and electromagnetic characteristics in Faraday-type MHD generator which was built in the MHD bypass scramjet. In Ref.[8] and Ref.[11], the potentials of the anode/cathode were set to be identical, which means all the anode/cathode are connected by wires, so the Hall current cannot be prevented. When setting boundary condition for the potential equation, not only the fixed value on the electrodes and zero value of the current density normal to wall on insulators should be satisfied, but also the current for the pair of electrodes connected to the same circuit should also be identical. This principle has not been embodied in these references. Soloviev, et al.[12] solved 2D and 3D linear electro-dynamic problems for solid and finely segmented electrodes for the special case when load factor is zero. The method does not consider the interaction between flow and magnetic-electric filed.

In this paper, the computational model consisting of Navier-Stokes (N-S) equations coupled with electrical-magnetic source terms, Maxwell equations and generalized Ohm's law is established for low magnetic Reynolds number Re_m magnetic-hydro flow in supersonic channels. Boundary conditions for the potential equation are set for the case when considering the Hall effect. The MHD channel with single-pair electrodes is numerically simulated, and the distributions of electrical parameters are studied. Then the MHD channel with five-pair electrodes is numerically simulated using the boundary condition setting rules established in this article, and Hall effect on the electrical-magnetic and flow parameters is analyzed. Performance of the MHD channel with continual electrodes, limited segmented electrodes and ideally segmented electrodes are compared.

2. Computation Model

2.1. Hydrodynamic equations

In the hypersonic inlet, temperature of the flow is low, and the ionization degree is quite low[13]. Even the most efficient ionization method electron beams is used to shoot from both sides of the channel, $Re_m \ll 1$ in the MHD channel. So in the MHD controlled scramjet engine, the flow is always the low Re_m flow. It is assumed that the gas is ideal and specific heat ratio is constant. The N-S equations coupled with electrical-magnetic source terms are

$$\frac{\partial \rho}{\partial t} + \nabla \cdot (\rho \boldsymbol{u}) = 0 \tag{1}$$

$$\frac{\partial (\rho \boldsymbol{u})}{\partial t} + \nabla \cdot (\rho \boldsymbol{u}\boldsymbol{u}) + \nabla p - \nabla \cdot \boldsymbol{\tau} = \boldsymbol{j} \times \boldsymbol{B} \tag{2}$$

$$\frac{\partial}{\partial t}\left[\rho(e_i + \frac{1}{2}u^2)\right] + \nabla \cdot \left[\rho(e_i + \frac{1}{2}u^2)\boldsymbol{u}\right] = \nabla \cdot (\boldsymbol{u} \cdot \boldsymbol{\tau} + \lambda \nabla T - p\boldsymbol{u}) + \boldsymbol{j} \cdot \boldsymbol{E} \tag{3}$$

where ρ is density of flow, $\boldsymbol{u}$ the flow velocity, $u=|\boldsymbol{u}|$, p the pressure, $\boldsymbol{\tau}$ the viscous stress tensor[14], $e_i = c_V T$ the inner energy of flow, c_V the specific heat at constant volume, T the temperature, λ the heat conduct coefficient, $\boldsymbol{j}$ the induce current density, $\boldsymbol{B}$ the magnetic induction strength, and $\boldsymbol{E}$ the electric field strength.

State equation is given as

$$p = \rho R T \tag{4}$$

2.2. Electrical-magnetic equations

Electrical-magnetic equations include Maxwell equations, electric current continuity equation and the generalized Ohm's law.

Maxwell equations are

$$\nabla \times \boldsymbol{H} = \boldsymbol{j} + \frac{\partial \boldsymbol{D}}{\partial t}, \quad \nabla \cdot \boldsymbol{B} = 0$$

$$\nabla \times \boldsymbol{E} = -\frac{\partial \boldsymbol{B}}{\partial t}, \quad \nabla \cdot \boldsymbol{D} = \rho_e$$

where magnetic field strength is given by $\boldsymbol{H}=\boldsymbol{B}/\mu$, and μ is magnetic permeability of the gas; Electric displacement vector $\boldsymbol{D}=\varepsilon \boldsymbol{E}$, and ε is permittivity; ρ_e is free charge density. In the MHD channel used for hypersonic vehicle, the flow velocity is much lower than the velocity of light, so the displacement current caused by the excess charge is much lower than the conduction current caused by the electric-magnetic induction. So, the displacement current term $\partial \boldsymbol{D}/\partial t$ in the Maxwell equation can be ignored. The magnetic Reynolds number ($Re_m = \mu \sigma u L$, σ is electrical conductivity, L is length) is very low ($Re_m \sim 10^{-3}$) in the MHD channel used for hypersonic vehicles, and the induction magnetic field caused by current is much lower than the applied magnetic field and can be ignored. The applied magnetic field is usually constant, so $\partial \boldsymbol{B}/\partial t = \boldsymbol{0}$. Maxwell equations can be simplified as

$$\nabla \times \boldsymbol{E} = \boldsymbol{0} \tag{5}$$

Current continuity equation is

$$\nabla \cdot \boldsymbol{j} = 0 \tag{6}$$

Generalized Ohm's law is

$$\boldsymbol{j} = \sigma(\boldsymbol{E} + \boldsymbol{u} \times \boldsymbol{B}) - \beta(\boldsymbol{j} \times \boldsymbol{b}) \tag{7}$$

where $\boldsymbol{b}=\boldsymbol{B}/B$, $B=|\boldsymbol{B}|$, and β is Hall parameter of electron. Ion slip term is ignored because Hall parameter of ion is much smaller than that of electron. According to Ref.[13], Hall parameter of ion is 40-300 times smaller than that of electron.

From Eq. (5), we can get $\boldsymbol{E}=-\nabla\varphi$, where φ is electric field potential. Combine Eq.(6) and Eq.(7) and we get the Poisson equation as

$$-\nabla \cdot (\sigma \nabla \varphi) = -\sigma[\nabla \cdot (\boldsymbol{u} \times \boldsymbol{B}) + \beta B \nabla \cdot \boldsymbol{u}] \tag{8}$$

In 2D channel, if $\boldsymbol{u} = [u \quad v \quad 0]$, $\boldsymbol{B} = [0 \quad 0 \quad B]$, $\boldsymbol{E} = [E_x \quad E_y \quad 0]$, then j_x and j_y can be expressed as

$$j_x = \frac{\sigma}{1+\beta^2}[(E_x + vB) - \beta(E_y - uB)] \tag{9}$$

$$j_y = \frac{\sigma}{1+\beta^2}[(E_y - uB) + \beta(E_x + vB)] \tag{10}$$

For supersonic MHD channel, the main performance parameters are enthalpy extraction ratio η_g and electrical efficiency η_e. The energy extraction ratio is defined as

$$\eta_g = w_g \big/ w_0$$

where $w_0=c_pT_0+u_0^2/2$ is energy of gas at inlet, c_p the specific heat at constant pressure and $w_g=W_g/\dot{m} = \int_0^L qA\mathrm{d}x \big/ \dot{m}$ the energy extracted from gas, q the energy extracting ratio, A the cross-sectional area of channel, $\dot{m}$ the mass flow rate. The electrical efficiency η_e is defined as

$$\eta_e = \frac{|\boldsymbol{E} \cdot \boldsymbol{j}|}{|\boldsymbol{u} \cdot (\boldsymbol{j} \times \boldsymbol{B})|} = \frac{|\boldsymbol{E} \cdot \boldsymbol{j}|}{|\boldsymbol{E} \cdot \boldsymbol{j}| + |\boldsymbol{j}^2/\sigma|} = \frac{-q}{-q+q_j}$$

where q_j is joule heat.

According to local analyses of MHD channel with continual or ideally segmented electrodes, $\eta_e = k$ can be get, where $k = E_y/(uB)$ is load factor of the MHD channel.

Past experience shows that Hall effect has serious influence on the MHD channel. The Hall parameter is defined as $\beta = eB/(m_e n k_c)$, where e is charge of electron, m_e the electron mass, n the number density of neutral particle, and k_c the electron scattering rate constant. From definition it can be seen that distribution of Hall parameter is related to the flow field. To simplify the computation we assume that Hall parameter is constant in the MHD interaction region.

3. Numerical Method and Boundary Conditions

3.1. Numerical method

Eqs.(1)-(4) and Eqs.(8)-(10) constitute complete resolving equations for the MHD channel, and are discredited by second order upwind format, and resolved by the implicit coupled solver.

3.2. Boundary conditions

For the N-S equations, pressure inlet is adopted for the inlet and the outlet, no-slip wall boundary is adopted and the wall temperature is set to be 1 000 K.

For segmented electrodes MHD channel, boundary conditions at electrodes for the potential equations are usually set by two methods. The first is to set the potential at electrodes, and usually set the potential at the anode/cathode to be the same; the second is to give current density distribution on the electrode according to experimental results. The dimensionless potential were set to be 1 and 0 on anode and cathode respectively in Ref.[8] and Ref.[11], which means all the anode/cathode were connected by wires and Hall current could not be prevented. In Ref.[15], j_y=const on electrode was assumed, and such current could be prevented from fleeing, but the current focusing effect could not be simulated. The method of giving the current density distribution on electrodes according to experimental results is costly and inconvenient[16].

In the present research effort, we will introduce a method to set boundary condition which is numerically viable and physically authentic.

For inlet, outlet, and insulated walls: $\boldsymbol{j}\cdot\boldsymbol{n}=0$.

For single-pair electrodes MHD channel, the electrode voltage is estimated through external load factor exploited in the algebraic model:

$$\Delta\varphi_y = E_y d_y = k u_0 B d_y$$

where d_y is distance between anode and cathode.

In MHD channel, due to Hall effect, the ions assemble at inlet and positive particles assemble at outlet, so Hall electric field is negative. That means the potential at upstream is always lower than downstream[13]. For segmented electrode MHD channel, boundary condition at electrodes must satisfy two conditions:

1) φ = const at electrode.

2) $\int_{i+} \boldsymbol{j} \cdot \boldsymbol{n} = \int_{i-} \boldsymbol{j} \cdot \boldsymbol{n}$, which means for the ith pair of electrodes connected to be one circuit, the current flow out of the cathode must be equal to the current flow into the anode.

The electrode voltage for one pair of electrodes is estimated by $\Delta\varphi_y=E_yd_y=ku_0Bd_y$, and the electrode voltage of the neighbor electrodes $\Delta\varphi_x=\varphi_{i+1}-\varphi_i$ is determined by Hall parameter. The function of segmented electrodes is to avoid Hall current, so we can assume that in the middle of two pairs of electrode, j_x=0.

From Eq. (9), we can get $E_x=\beta(E_y-uB)$, so

$$\Delta\varphi_x = E_x d_x = \beta(\Delta\varphi_y / d_y - uB) d_x \tag{11}$$

where d_x is distance between the neighbor electrodes.

4. Computational Model Validation

4.1. Hartmann flow

Theoretically, internal flow in the MHD generator

belongs to the Hartmann flow[17], which is one of the basic important flows having the analytical solution. So, the Hartmann flow can be used to verify the computational model[18]. The size of channel is 20 mm× 10 mm×2 mm, and that of the grid is 20×10×50, Re=100, Re_m=1.5×10^{-4}. Under these conditions, ratio of the induced magnetic induction to the applied magnetic induction is of magnitude of 10^{-5} and can be ignored. In order to make the flow steady enough, the periodic boundary condition is adopted. Fig.1 shows the comparison of analytical solution and numerical solution, and it is obvious that they are totally coincident. In Fig.1, Ha is Hartmann number.

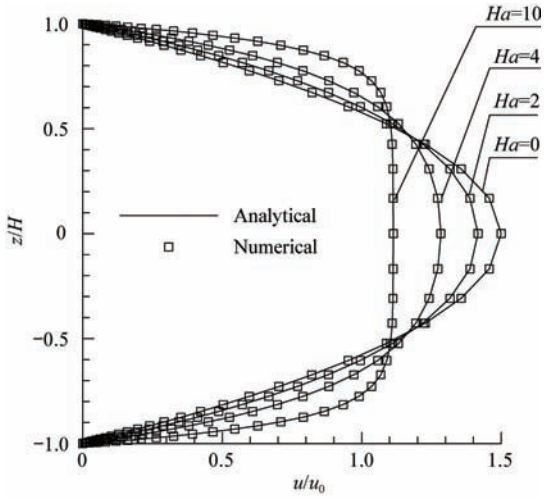

Fig.1 Velocity profile at different Hartmann numbers.

4.2. Comparison with experiment

Ioffe Physico-Technical Institute of the Russian Academy of Science cooperated with the Johns Hopkins University, and they studied the problem of gas flow controlled by a magnetic field as applied to flows in intakes of supersonic aircraft using inert gas as working body, and the feasibility of controlling the shock wave by MHD was demonstrated experimentally[19-21]. In this experiment, the external electric field has to be applied along the direction of the electromotive force direction in order to decelerate the flow because of large near-wall potential drop.

In the present research, parameters of Ref.[20] are adopted to calculate the flow: the working gas is Kr, Ma_0=4.3, T_0=1 550 K, ρ_0=6.45×10^{-2} kg/m^3, σ_0= 1 200 S/m, u_0=2.1×10^3 m/s. Near-wall potential drop is not considered, and the setting U_3=U_4=U_5=U_6=6 V was made as shown in Fig.2, where 1-7 are numbers of electrodes. The geometry parameters of model are set according to Ref.[19].

Fig.3 gives the comparison between numerical results and experimental results, and shows the distance of intersection of oblique shocks, arising from leading edges of the diffuser walls, versus induction of applied magnetic field. When B=0 T and U=0 V, we get x_c = 42 mm, which is in accordance with experimental data. In the experiment, orientation of the applied electric field is along the electromotive force direction, i.e. $j=-\sigma(E+uB)$, so the extent of decelerating the flow is more obvious. While in the computational model, orientation of the applied electric field is reverse to the electromotive force direction, i.e. $j=-\sigma(-E+uB)$. When electric voltage is applied and B=0, the flow is decelerated by joule heating and energy input, so x_c<42 mm. When B=0.1 T, upstream channel is in generator mode and the flow is decelerated; while downstream channel is in accelerator mode and the flow is accelerated, so $x_c|_{B=0.1T}>x_c|_{B=0\ T}$. When B>0.1 T the whole channel is in the generator mode, and x_c is decreased.

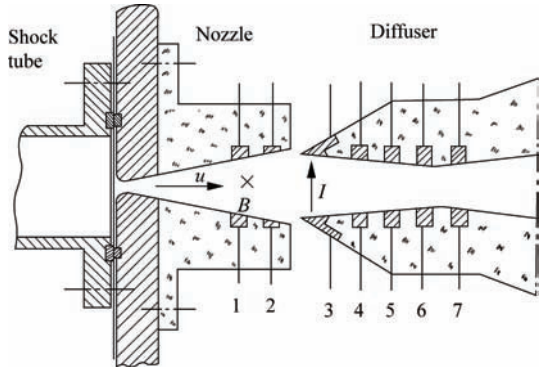

Fig.2 Scheme of MHD channel with electrodes used in experiment.

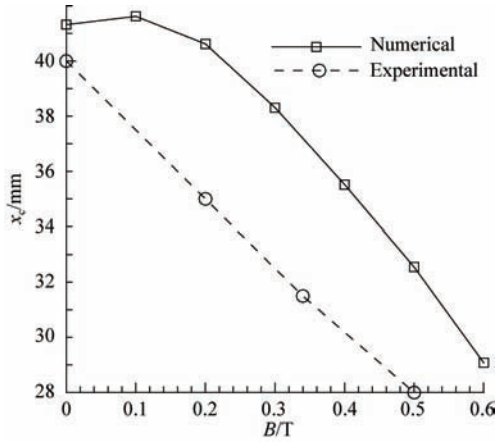

Fig.3 Position of shock intersection point vs induction of applied magnetic field.

Due to the lack of specific experimental data, difference of direction of the applied electric field, and uncertainty of some parameters in experiment, numerical result is different from experimental result to some extent, but the whole trend is the same, i.e., intersection point of the shock waves moves upstream as B increases.

5. Simulation of MHD Channel

5.1. Simulation of single-pair electrodes MHD channel

Fig.4 shows the geometry of single-pair electrodes MHD channel with its size being 0.1 m×0.1 m, and the width of electrode is 0.04 m. The velocity $\boldsymbol{u}$ is along x

direction, and the magnetic induction $\boldsymbol{B}$ along z axis. The size of grid is 110×120.

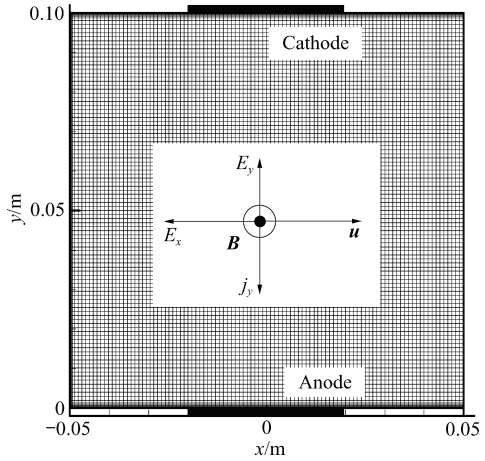

Fig.4 Geometry and grid structure of single-pair electrodes MHD channel.

The inlet flow conditions are set to be T_0=1 000 K, p_0=1.0×10^5 Pa, Ma_0=4. Conductivity is set to be uniform with value of σ=20 S/m. The magnetic induction is set to be uniform with B=0.5 T. The magnetic interaction number, which is defined as the ratio of magnetic body force to the fluid inertia force, is $Q=\sigma_\infty B_\infty^2 L/(\rho_\infty u_\infty)$=2.77×10^{-4}, which implies that electrical magnetic force has little effect on flow parameters. The electrode voltage is estimated by $\Delta\varphi_y = E_y d_y = k u_0 B d_y$, and is set as k=0.5 when B=0.5 T, $\Delta\varphi_y$ = 60 V. Potential on anode is φ_+=30 V and potential on cathode is φ_-= −30 V.

When β = 0, the current distribution and the potential distribution are shown in Fig.5. Fig.5(a) shows the current lines, in which the current flows from cathode to anode, and concentrates at the ends of electrodes. Fig.5(b) shows the distribution of the current density, and it is observed that the value is higher in the vicinity of electrode ends and is lower at inlet and outlet corners. Potential distribution is shown in Fig.5(c), and it is evident that the potential near the insulators is higher than that of electrodes. When the plasma flows through the MHD channel, the positive particles move towards

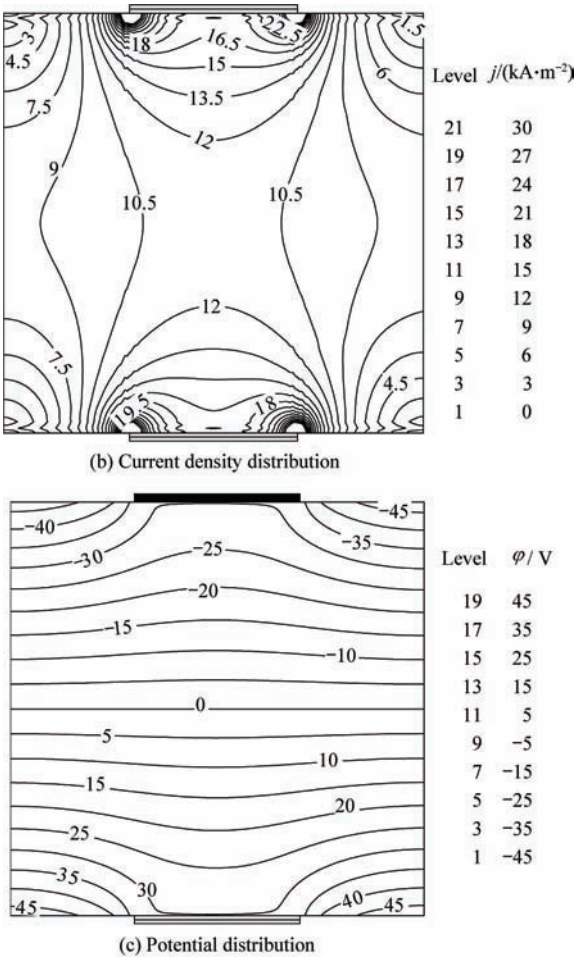

Fig.5 Current and potential distribution when β = 0.

lower wall of channel and negative particles move towards upper wall due to the Lorentz force, so electrical field $\boldsymbol{E}$ pointing to upper wall is introduced. When connecting the electrodes to circuit, the current flows to release some accumulated charges, so the voltage between the electrodes is lower than that of the insulators. The computational result proves to be consistent with theoretical analysis. As Hall effect is not considered in this case, the distributions of both the current and potential are symmetrical about line x=0.

Fig.6 depicts the current and potential distribution

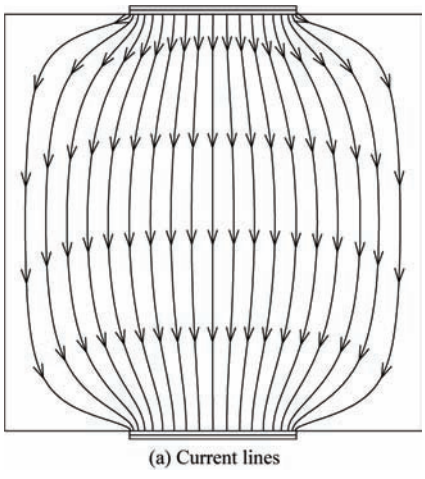

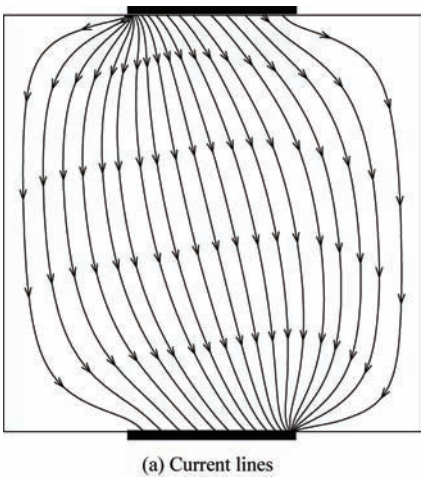

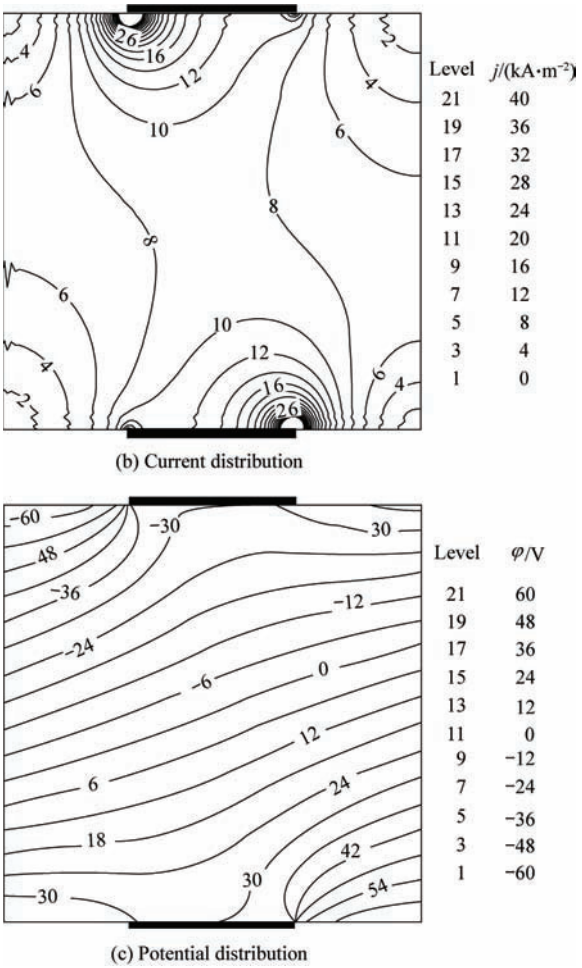

Fig.6 Current and potential distribution when $\beta = 1.0$.

when $\beta = 1.0$. It is shown that the Hall effect contributes to the asymmetry of both the distribution of the current and potential, and the current density concentrates at the upper end of the cathode and the lower end of the anode. Hall electric field pointing to the upper stream can be seen in Fig.6(c).

5.2. Simulation of five-pair electrodes MHD channel

The channel geometry is similar to that in Ref.[11]. As shown in Fig.7, the size is 0.2 m×0.04 m and electrode width is 0.02 m. The incoming flow condition is the same as that in Section 5.1 and the grid size is 205×50.

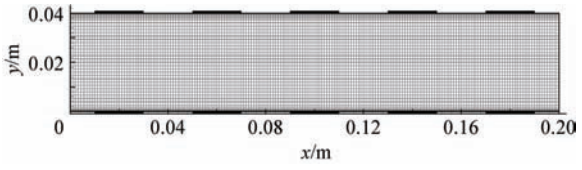

Fig.7 Geometry and grid of five-pair electrodes MHD channel.

Fig.8 shows the Mach number and pressure distribution of channel when B=0 T. Boundary layer development can be observed in Fig.8(a). Effective flow area is decreased by the boundary layer, so the flow is compressed. The compression waves are observed as shown in Fig.8(b).

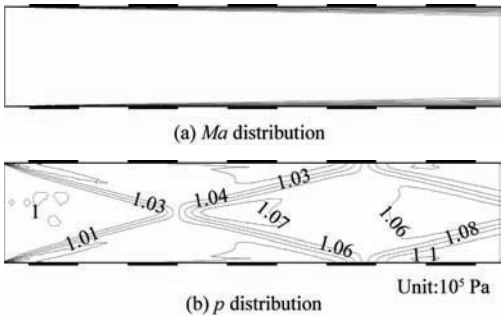

Fig.8 Mach number and pressure distribution when B=0 T.

Figs.9(a)-9(c) show the current and potential distribution when B=8 T and $\beta = 0$, and the electrode voltage is $\Delta\varphi_y$=300 V and accordingly $\bar{k} = 0.52$. The magnetic interaction number $Q = \sigma_\infty B_\infty^2 L/(\rho_\infty u_\infty) = 0.29$, which means that the electrical magnetic force has an obvious effect on the flow parameters. In Fig.9(a), the current flows from cathode into the corresponding anode, which is connected to the same circuit. Fig.9(b) shows that the current density clusters at the ends of electrodes and is symmetrical about center line of the channel y=0.2 m. The current density is decreased along the flow direction because the flow parameter is changed due to the magnetic-electrical effect. It is shown in Fig.9(c) that the potential distribution is symmetrical about center line of the channel and line x=0.1 m.

Fig.9(d) shows the joule heating distribution along the wall. Without Hall effect, joule heating distributions of the upper and lower wall are the same. It is shown that joule heating distribution is consistent with current density distribution on walls; and values on electrode ends are much higher than the average value, which may introduce cooling problems.

Figs.9(e)-9(f) show the Mach number and pressure distribution when B=8 T and $\beta = 0$. It is obvious that the Mach number decreases along x axis as a result of

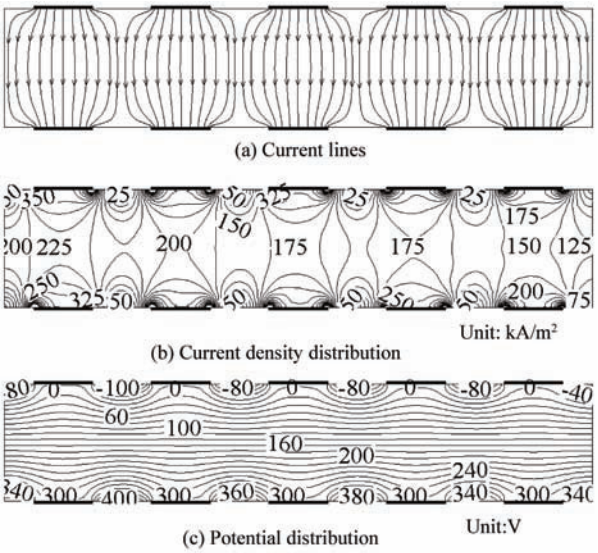

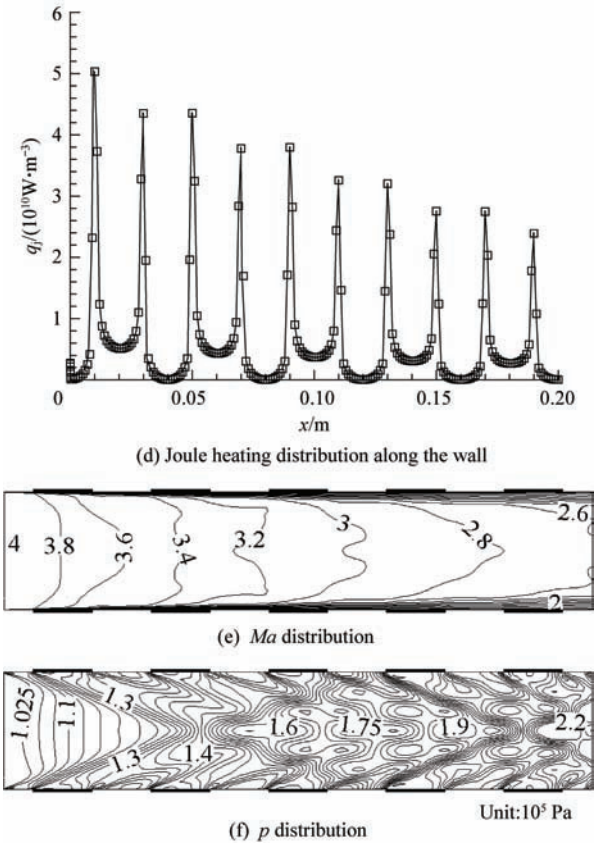

Fig.9 Parameter distributions when B=8 T and β = 0.

MHD effect, while pressure increases along x axis. It is shown in Fig.9(f) that waves arise from the ends of electrodes, and become a complicated wave system. Both *Ma* and *p* distributions are symmetrical about center line of the channel.

When B=8 T and β = 0.5, the electrode voltage is $\Delta\varphi_y$=300 V and $\Delta\varphi_x$=120 V according to the method described in Section 2.2. So the potential of electrodes on upper wall is 0, 120, 240, 360, 480 V respectively, and the potential of electrodes on lower wall is 300, 420, 540, 660, 780 V respectively. Figs.10(a)-10(c) show the distributions of current and potential. It is shown that the distributions are asymmetrical due to Hall effect, and Hall electrical field pointing towards inlet direction is obvious. Fig.10(d) shows the joule heating on upper and lower walls. The Mach number and pressure distribution are shown in Figs.10(e)-10(f)

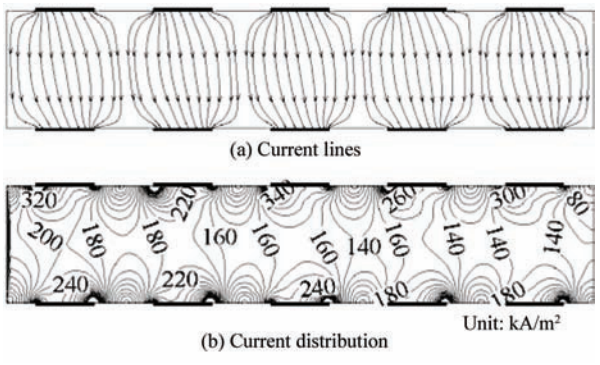

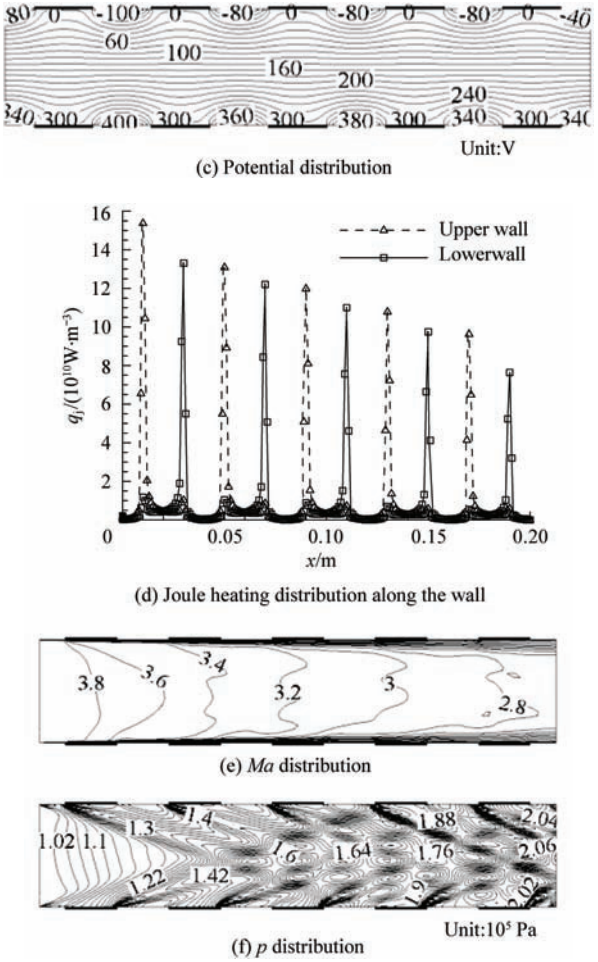

Fig.10 Parameters distributions when B=8 T and β = 0.5.

respectively. Due to the Hall Effect, the distributions are asymmetrical.

5.3. Comparison of performance of different MHD channels

Performance of the continual electrode MHD channel is deteriorated due to Hall effect and joule heating. In order to alleviate the disadvantage of Hall effect, segmented electrode can be used. For ideally segmented electrode MHD channel, disadvantage of Hall effect can be eliminated theoretically, and the Hall current is 0. Confined by electrode fabricating techniques and the material performance, the electrode cannot be segmented infinitely in practice, and finite segmented electrode is usually adopted instead. In this section, different kinds of MHD channels will be compared.

Using the geometry of last section, the following values are set: B=8 T, σ=20 S/m, $\Delta\varphi_y$=300 V. The results are listed in Table 1. It is shown that performance of ideally segmented electrode is the best. When β = 0.5, performance of continual electrode MHD channel is better than that of five-pair electrodes MHD channel and worse than that of ten-pair electrodes MHD channel. When β>1.0, performance of five-pair electrodes MHD channel is better than that of continual

Table 1 Performance parameters of different kinds of channels

Type of channel	β	$\bar{k}$	Ma_2	p_2/MPa	T_{max}/K	$\bar{q}$ /(10^9W·m^{-3})	$\bar{q}_j$ /(10^9W·m^{-3})	η_g/%	η
Without MHD			3.84	0.108	2 257				
Ideally segmented electrode		0.42	2.28	0.243	2 476	1.54	2.16	8.28	0.417
Continual electrode	0.5	0.41	2.46	0.219	2 541	1.31	1.88	7.04	0.410
	1.0	0.39	2.78	0.183	2 749	0.92	1.39	4.92	0.398
Five-pair electrodes	0.5	0.53	2.59	0.206	4 309	1.19	1.73	6.36	0.407
	1.0	0.55	2.79	0.185	5 000	1.02	1.44	5.49	0.416
Ten-pair electrodes	0.5	0.48	2.37	0.219	3 681	1.33	1.90	7.13	0.412
	1.0	0.50	2.55	0.196	4 561	1.22	1.76	6.57	0.411

electrodes MHD channel and worse than that of ten-pair electrodes MHD channel. It can be concluded that with the increase of β, the advantage of the segmented electrode MHD channel will become more obvious; performance of segmented electrode MHD channel is better when more electrodes are used.

It should be noted that, when β=1.0, the highest temperature in the five-pair electrodes MHD channel reaches 5 000 K, which will introduce difficulty to cooling system. The high temperature near electrode is due to the current cluster at the ends of electrodes, which leads to high joule heating. High joule heating at the ends of electrodes causes not only high temperature but also complicated waves in the channel. The reason for the current cluster mainly lies in two aspects.

1) The current between insulators comes into electrodes;

2) Hall effect makes the current cluster at upper point of cathodes and lower point of anodes. Making the electrode segmentation finer can alleviate the problems.

6. Conclusions

(1) Using the boundary condition given method derived in this paper, the current flow phenomenon in the MHD channel can be simulated correctly.

(2) The Hall effect makes the current concentrate at the upper ends of cathodes and lower ends of anodes, causing the flow to be asymmetrical.

(3) When magnetic interaction number is 0.29, MHD has an obvious effect on the flow field: decreasing Mach number, increasing pressure and introducing complicated waves to the channel.

(4) With the increase of β, the advantage of the segmented electrode MHD channel is more obvious; performance of segmented electrode MHD channel is better if segmentation of electrode is finer. But in the finite segmented electrode MHD channel, there exist local high temperature and complicated waves, helping the electrode segmentation finer alleviate the problems.

References

[1] Resler E L, Sears W R. The prospects for magneto-aerodynamics. Journal of the Aeronautical Sciences 1958; 25(4): 235-245.

[2] Ziemer R W. Experimental investigation in magneto-aerodynamics. American Rocket Society 1959; 29: 642-672.

[3] Gurijanov E P, Harsha P T. AJAX: new directions in hypersonic technology. AIAA-1996-4609, 1996.

[4] Freishtadt V L, Kuranov A L, Sheikin E G. Use of MHD systems in hypersonic aircraft. Technical Physics 1998; 43(11): 1309-1313.

[5] Kuranov A L, Sheikin E G. Magnetohydrodynamic control on hypersonic aircraft under "AJAX" concept. Journal of Spacecraft and Rockets 2003; 40(2): 174-182.

[6] Golovachov Y P, Sushchikh S Y, van Wie D M. Numerical simulation of MGD flows in supersonic inlets. AIAA-2000-2666, 2000.

[7] Golovachov Y P, Kurakin Y A, Schmidt A A, et al. Numerical investigation of non-equilibrium MGD flows in supersonic intakes. AIAA-2001-2883, 2001.

[8] Gaitonde D V, Poggie J. Elements of a numerical procedure for a 3-D MGD flow control analysis. AIAA-2002-0198, 2002.

[9] Gaitonde D V. Magnetohydrodynamic energy-bypass procedure in a three-dimensional scramjet. Journal of Propulsion and Power 2006; 22(3): 498-510.

[10] Gaitonde D V. Effect of Hall currents on simulated three-dimensional scramjet with magnetohydrodynamic bypass. Journal of Propulsion and Power 2006; 22(3): 700-703.

[11] Lu H Y. Conceptual study on integrated design of airframe/MHD bypass scramjet for a waverider-based hypersonic vehicle. Ph.D. thesis, School of Aeronautic Science and Engineering, Beihang University, 2008. [in Chinese]

[12] Soloviev V R, Krivtsov V M, Konchakov A M, et al. E-beam plasmas 2-D and 3-D analysis in magnetohydrodynamic applications. AIAA-2004-183, 2004.

[13] Ju Z X, Lu Y C, Jing H B. Open cycle MHD power generation. Beijing: Beijing University of Technology Press, 1998; 45-65. [in Chinese]

[14] Anderson J D. Computational fluid dynamics—the basic applications. Columbus, OH: McGraw-Hill Company, 1995.

[15] Zheng X M, Xu D J, Cai G B. Numerical simulation of the two-dimensional MHD controlled inlet. Journal of Aerospace Power 2009; 24(3): 581-587. [in Chinese]

[16] Gotoh D, Takahashi T, Fujino T, et al. Computational analysis of HVEPS scramjet MHD power generation.

AIAA-2007-4015, 2007.
[17] Sutton G W, Sherman A. Engineering magnetohydrodynamics. New York: Mcgraw-Hill Book Company, 1965.
[18] Lu H Y, Lee C H, Dong H T. Characterization of the three-dimensional supersonic flow for the MHD generator. Science in China Series G: Physics Mechanics Astronomy 2009; 52(4): 534-545.
[19] Bobashev S V, Golovachov Y P, van Wie D M. Deceleration of supersonic plasma flow by an applied magnetic field. Journal of Propulsion and Power 2003; 19(4): 538-546.
[20] Bobashev S V, Erofeev A V, Lapushkina T A, et al. Experiments on MHD control of attached shocks in diffuser. AIAA-2003-169, 2003.
[21] Bobashev S V, Erofeev A V, Lapushkina T A, et al. Recent results on MHD flow control at Ioffe institute. AIAA-2006-8012, 2006.

Biographies:

ZHENG Xiaomei Born in 1982, She received B.S. and Ph.D. degrees from Beihang University in 2004 and 2010 respectively, and then became an engineer of Beijing Aeronautical Engineering Technical Research Center. Her main research interest is application of MHD technology in hypersonic vehicles.
E-mail: cherry@sa.buaa.edu.cn

LU Haoyu Born in 1978, He received B.S. and Ph.D. degrees from Beihang University in 2001 and 2008 respectively, and now is a lecturer of Beihang University. His main research interests are application of MHD technology to hypersonic vehicles, MHD numerical method and space physics as well.
E-mail: Lvhy@buaa.edu.cn

XU Dajun Born in 1977, He received B.S. and Ph.D. degrees from Beihang University in 1999 and 2007 respectively, and now is a lecturer of Beihang University. His main research interest is spacecraft and launch vehicle conceptual design.
E-mail: xdj@buaa.edu.cn

CAI Guobiao Born in 1967, He received B.S. and Ph.D. from Beihang University in 1989 and 1996 respectively, and now is a professor of Beihang University. His main research interests are vacuum plume effect and control technology, rocket engine optimum design and simulation technology, hybrid rocket engine technology and application.
E-mail: cgb@buaa.edu.cn